PCCP

Accepted Manuscript

This is an *Accepted Manuscript*, which has been through the Royal Society of Chemistry peer review process and has been accepted for publication.

Accepted Manuscripts are published online shortly after acceptance, before technical editing, formatting and proof reading. Using this free service, authors can make their results available to the community, in citable form, before we publish the edited article. We will replace this *Accepted Manuscript* with the edited and formatted *Advance Article* as soon as it is available.

You can find more information about *Accepted Manuscripts* in the **Information for Authors**.

Please note that technical editing may introduce minor changes to the text and/or graphics, which may alter content. The journal's standard **Terms & Conditions** and the **Ethical guidelines** still apply. In no event shall the Royal Society of Chemistry be held responsible for any errors or omissions in this *Accepted Manuscript* or any consequences arising from the use of any information it contains.

ARTICLE TYPE

Catalytic Activity of Pd-doped Cu Nanoparticles for Hydrogenation as a Single-Atom-Alloy Catalyst

Xinrui Cao,[a] **Qiang Fu,**[*a] **and Yi Luo**[ab]

The single atom alloy of extended surfaces is known to provide remarkably enhanced catalytic performance toward heterogeneous hydrogenation. Here we demonstrate from first principles calculations that this approach can be extended to nanostructures, such as bimetallic nanoparticles. The catalytic properties of the single-Pd-doped Cu_{55} nanoparticles have been systemically examined for H_2 dissociation as well as H atom adsorption and diffusion, following the concept of single atom alloy. It is found that doping a single Pd atom at the edge site of Cu_{55} shell can considerably reduce the activation energy of H_2 dissociation, while the single Pd atom doped at the top site or in the inner layers is much less effective. On Cu_{55} the H atom adsorption is slightly stronger than that on the Cu(111) surface; however, a larger nanoparticle that contains 147 atoms could effectively recover the weak binding of the H atoms. We have also investigated the H atom diffusion on the 55-atom nanoparticle and found that spillover of the produced H atoms could be a feasible process thanks to the low diffusion barriers. Our results have demonstrated that facile H_2 dissociation and weak H atom adsorption could be combined at the nanoscale. Moreover, the effects of doping one more Pd atom have also been investigated on the H_2 dissociation and H atom adsorption. We have found that both the doping Pd atoms in the most stable configuration could independently exhibit their catalytic activity, behaving as two single-atom-alloy catalysts.

1 Introduction

A catalyst is such a substance that can be used to improve the rate or selectivity of the chemical reactions. It is closely related to our daily lives from producing fuels and pharmaceutical, to the elimination of pollution. Transition metals are well known, among the various catalysts, for their remarkable catalytic properties in chemical industries[1]. Their catalytic properties are originated from the particular electronic structures and can be well interpreted within the framework of the *d* band model, that is, the adsorbate-substrate interaction increases with the upshift of the d states[2–4]. Recently, the bimetallic alloys of transition metals aroused great interests because of their superior catalytic activities with respect to the ones of the pure constituent elements[5–10]. For instance, it was experimentally demonstrated that the $Pt_3Ni(111)$ alloy is 10-fold more active than the corresponding Pt(111) surface in the catalysis of the oxygen reduction reaction (ORR)[5]. Through the ligand (electronic interaction between different elements) and the strain (changes in the lattice constant) effects, transition metal alloying provides a very effective way to tune the d states, and thus offers great promise for the improvement of

the catalytic properties[11].

In the description of a catalytic reaction cycle, the adsorption energies (E_{ad}) and the transition-state energies (E_{TS}) are the key values of understanding the catalytic processes. The constraint of the Brønsted-Evans-Polanyi (BEP) relations, however, makes it challenging to independently change these two types of energies, because the thermodynamic binding energies and the kinetically relevant activation energy barriers are correlated[12–15]. A facile bond-breaking process usually corresponds to a difficult desorption of products, and vice versa, and causes the reaction rate always limited to one of these two steps. The concept of near-surface alloy (NSA), in which a full monolayer of solute component is placed in the first subsurface layer of the host metal, represents a breakthrough in the rational catalysis design beyond such constraint[16,17]. It was found that some of the NSAs incorporate weak hydrogen adsorption (a low E_{ad} value) with easy H_2 dissociation (a low E_{TS} value) at the same time[16], behaving as "*outliers*" in the corresponding BEP relationship[18].

Recently, the concept of single atom alloy (SAA), in which a small amount of precious metal is doped into the common low-cost host[19–21], was proposed as another type of "outliers" in the catalysis of hydrogenation[18,22]. It was experimentally verified that alloying one percent of Pd atoms can significantly promote the H_2 dissociation, and at the same time, does not strongly bond the resulting hydrogen atoms[19,22]. As a result, the hydrogenation reaction can be catalyzed in a very

---
[a] *Department of Theoretical Chemistry and Biology, School of Biotechnology, Royal Institute of Technology, S-106 91 Stockholm, Sweden. Tel: 0046-8-55378407; E-mail: qfu@kth.se*
[b] *Hefei National Laboratory for Physical Sciences at the Microscale, University of Science and Technology of China, Hefei 230026, Anhui, P. R. China*

effective and selective way. In addition, such approach offers additional benefit of cost, because the expensive palladium atoms need only to be doped in a very low concentration [19,22]. Our previous theoretical studies have compared the activation energies of H_2 dissociation between flat (111) and stepped (211) surfaces, and found that alloying Pd atoms at the step edge is more effective to promote the dissociation of H_2 molecule [23]. In fact, nanoparticles usually contain low-coordinated structures such as steps on their surfaces; thus it is interesting to investigate the applicability of the SAA concept [22] at the nanoscale. It is worth noting that such idea has also been proposed in a recent experiment [24].

In this study, we have performed first-principles calculations to investigate the catalytic properties of the single-Pd-doped Cu nanoparticles toward heterogeneous hydrogenation, following the concept of single atom alloy on the extended surfaces. A 55-atom icosahedral cluster is used to represent the Cu nanoparticles. The H_2 dissociation, H atom adsorption and diffusion have been systematically investigated. In addition, the effects of doping one more Pd atom have also been studied. Our results clearly demonstrated that the concept of single atom alloy is effective and can be extended to the nanoscale.

2 Computational Details

Our calculations were performed with spin-polarized density functional theory (DFT). The effects of spin polarization were found to be negligible. The electron-ion interaction was described by the projector augmented wave (PAW) pseudopotentials [25]. The energy cutoff for the plane-wave basis set was set to be 400 eV. The exchange-correlation interactions were described by GGA-PW91 [26]. A three-dimensional (3D) periodic cube supercell with a 25 Å (30 Å for the larger cluster) lattice constant was used in the calculations. In this case, distance between the two clusters in neighboring supercells was large enough. The Brillouin zone sampling was carried out using the Γ point. All the atoms were allowed to relax until the maximum force becomes less than 0.02 eV/Å. The climbing-image nudged elastic band (CI-NEB) method [27] was used to find the transition state of H_2 dissociation and H atom diffusion. The Dimer method [28] was employed to verify the saddle point obtained by the CI-NEB method. All the calculations were performed by using the Vienna ab-initio simulation package (VASP) [29,30].

3 Results and Discussion

3.1 Structure of the Cluster Model

An icosahedral cluster with 55 atoms, shown in Figure 1, is chosen as a model system to examine the catalytic activity of
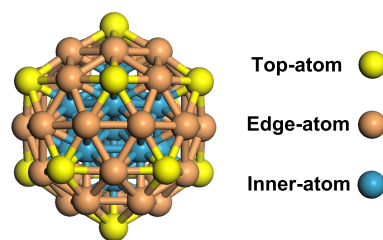

Fig. 1 Schematic structure of the icosahedral Cu_{55} cluster used in our calculations. The two kinds of inequivalent Cu atoms at the shell of the cluster, namely the top atom and the edge atom, are shown in different colors.

the nanoparticles. This cluster, having a diameter of about 1 nm, is highly symmetrical and enclosed by twenty {111} facets. It is well known that the close-packed {111} facet has the lowest surface energy [31,32], making it commonly exist at the surface of the nanoparticles. Previous calculations have shown that the most stable configuration of the Cu_{55} cluster is the second Mackay icosahedron [33], and this finding has also been verified by different experiments [34,35]. These results indicate that our selected polyhedral icosahedron can represent the true geometry of the Cu_{55} cluster. Moreover, since the surface of the icosahedral cluster is only enclosed by the {111} facet, its catalytic activity can be well compared with our previous results for the flat and stepped (111) extended surfaces [23].

It can be seen that there are two kinds of inequivalent atoms, that is, the edge atom and the top atom (see Figure 1), at the shell of the 55-atom nanoparticle. Because Pd has a larger lattice constant than Cu, doping Pd atom will cause distortion in the relaxed icosahedral nanoparticles. We show the detailed distortion of the single-Pd-doped Cu_{55} nanoparticles in Figure 2. One can see that in the pure Cu_{55} there are two non-equivalent Cu-Cu bonds, i.e. the Cu^{top}-Cu^{edge} and the Cu^{edge}-Cu^{edge} bond, with its bond length 2.53 and 2.60 Å respectively. After doping one Pd atom at the top site, the Pd^{top}-Cu^{edge} bond length increases to 2.61 Å, while other bond lengths are basically unchanged. It means that doping a single Pd atom at the top site causes local distortion. However, the situation changes when the Pd atom is doped at the edge site. One can see that at this site the doping Pd atom induces a significant deformation of the nearby Cu atoms, which could further affect the electronic structure of the Pd atom.

3.2 H_2 Dissociation on the Pure and Single-Pd-Doped Cu_{55} Nanoparticles

First we investigate the effects of doping one Pd atom on the dissociation of the H_2 molecule. On the edge site we have considered several possible pathways for the H_2 dissociation, and finally we identified two representative ones, as given in Figure 3. The adsorption energy of the H_2 molecule and the
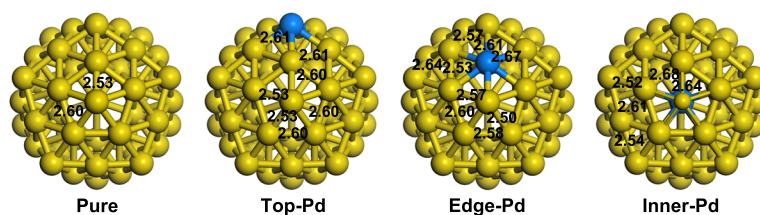
Fig. 2 The metal-metal distances in the pure and single-Pd-doped Cu_{55} nanoparticles (unit: Å). Only the important bond lengths are listed. Because of the high symmetry of the nanoparticles, the length of the equivalent metal-metal bond is not shown.

activation energy of H_2 dissociation are listed in Table 1. We found that H_2 adsorption does not cause remarkable distortion in the single-Pd-doped nanoparticles, with the maximum change of the metal-metal distance less than 0.05 Å. The initial state with H_2 molecule being far away from the cluster is chosen as the zero reference point, and the activation energy is defined as the energy difference between the transition state and this initial state. It is worth noting that such definition comes from the classic work of Lennard-Jones when he tried to explain the spontaneous activated (dissociative) adsorption of H_2 molecule on the nickel surface[36], and is still widely used when discussing the adsorption and dissociation of H_2 molecule on metal surface[37,38]. In path a the H_2 molecule is aligned parallel to the edge between the two triangles of the {111} facets, while in path b the H_2 rotates by 90° and is perpendicular to the edge. The activation energy of the H_2 dissociation is -0.01 and 0.07 eV respectively for the path a and b. We also investigated the H_2 dissociation on the pure icosahedral Cu_{55} cluster, and found the corresponding activation energy up to 0.45 eV. From these results one can see that doping only one Pd atom at the edge site of Cu_{55} can significantly promote the dissociation of the H_2 molecule. It is worth noting that the reduction of activation energy by doping one Pd atom is more effective on Cu_{55} nanoparticle (-0.01 eV) than on the flat and stepped Cu(111) surfaces (0.29 eV and 0.05 eV respectively), as was indicated in our previous calculations[23].

We now consider the H_2 dissociation when Pd atom is doped at the top site (shown in Figure 4). The calculated adsorption energy and activation energy are listed in Table 1. At this top site the activation energy is found to be 0.65 eV, which is even higher than that on the edge site of the pure Cu_{55} cluster (0.45 eV). Nevertheless, in comparison with the value at the top site of the pure Cu_{55} (0.99 eV), such a doping has also reduced the activation energy, although it is still too high to dissociate the H_2 molecules. The activation energy difference at the top and edge doping sites can be interpreted by the difference of the local configurations, which comes from the cooperative effect of the neighboring Cu atoms for the stabilization of the corresponding transition state. We take the comparison between the path a in Figure 3 and the path in Figure 4 as the example. In the former case, the distance between the hydrogen
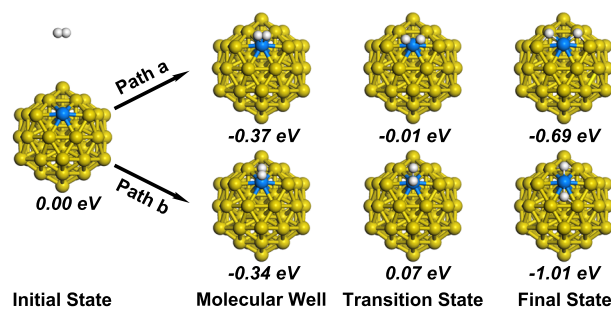
Fig. 3 The two representative pathways of H_2 dissociation after doping a single Pd atom at the edge site of Cu_{55}. The activation energy is -0.01 and 0.07 eV for path a and b respectively. The yellow and blue atoms represent Cu and Pd atoms.
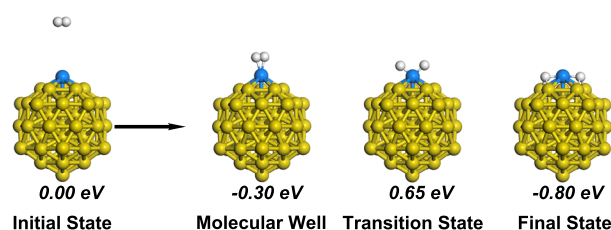
Fig. 4 Dissociation pathway of H_2 molecule after doping a single Pd atom at the top site of Cu_{55}. The activation energy is 0.65 eV compared with the initial state.

and the neighboring Cu atom is 3.0 Å at the molecular well (the adsorbed dihydrogen structure). In order to approach the two Cu atoms, the distance between the two hydrogen atoms prolongs to only 1.47 Å at the saddle point. However, in the latter case, the hydrogen-copper distance becomes 3.7 Å at the molecular well. Thus the distance between the two hydrogen atoms has to be as long as 2.38 Å at the saddle point in order to approach these Cu atoms, resulting in a significant increase of the corresponding activation energy. The above results demonstrate that doping one Pd atom at the top site of Cu_{55} cannot promote the dissociation of the H_2 molecules. As a result, in the following investigations, we will not consider such doping pattern as the active site for H_2 dissociation.

We then turn our attention to the effects of inter-layer doping on H_2 dissociation by replacing one inter-layer Cu atom with Pd. Here, only the dissociation pathway with the lowest activation energy, similar to the path a in Figure 3, is discussed. From the results (Table 1) we found that substituting one Pd atom at the inner layer could reduce the activation energy to some extent (from 0.45 eV to 0.36 eV), but much less effective than Pd-doping at the surface layer. This situation is quite similar to what has been found for the subsurface substitution at the flat Cu(111) surfaces[23]. In addition, we considered the case of doping one Pd atom at the center of the Cu_{55} cluster, and found that the activation energy of H_2 dissociation cannot be reduced. Instead, the value increases to 0.51 eV compared to the corresponding value of the pure Cu_{55} cluster (Table 1).

3.3 H Atom Adsorption on the Pure and Single-Pd-Doped Cu_{55} Nanoparticles

It should be noted that as a superior catalysis for hydrogenation, only having a low activation energy of H_2 dissociation is far from enough. In addition, the Pd-doped Cu nanoparticles should not bond the resulting hydrogen atoms too strongly. As a result, the H atom adsorption energies were also investigated, with the configuration and adsorption energy shown in Figure 5 and Table 2 respectively.

There are two kinds of hollow sites for H atom adsorption, that is, the hcp and the fcc site, on the surface of the Cu_{55} nanoparticle (Figure 1). By comparing the $E_{ad}(H)$ values between the configuration a (or c) and b (or d) (see Figure 5), one can see that on Cu_{55} the $E_{ad}(H)$ at the fcc site is about 0.13 eV higher than that at the hcp site, regardless of Pd atom doping. We then compare the $E_{ad}(H)$ values between the pure (a,b) and the single-Pd-doped (c,d) Cu_{55} nanoparticles. It can be seen that the adsorption energy increases by 0.10 eV after doping one Pd atom. It is worth noting that the effect of Pd atom on the $E_{ad}(H)$ is qualitatively local, because when the H atom does not directly bond with the Pd atom, as in the configurations e - h (hcp sites), the $E_{ad}(H)$ values are closer to that on the pure Cu_{55}. We also investigated the case in which the H atom is far away from the Pd atom, that is, locating at the other side of the cluster, and found that the $E_{ad}(H)$ value is 2.70 and 2.54 eV respectively at the fcc and the hcp site. In that case, the adsorption energy is almost the same as that on the pure Cu_{55} nanoparticle.

Although doping a single Pd atom does not significantly increase $E_{ad}(H)$, the absolute value of the adsorption energy is still an issue of great concern. As has been mentioned, in order to increase the selectivity of the hydrogenation reactions, a good SAA should not bind the H atoms too strongly. Compared to Cu(111), however, the Cu_{55} nanoparticle might have a stronger affinity to the H atoms, because of a lower coordi-
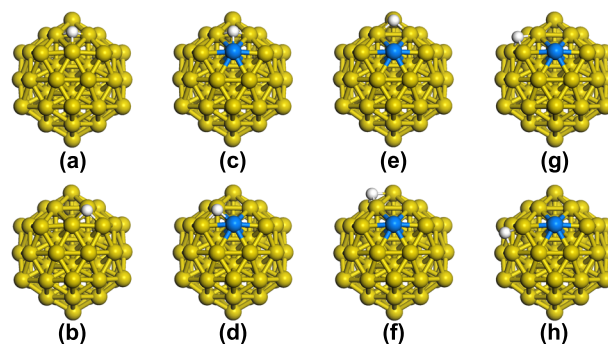
Fig. 5 The adsorption configurations of a single H atom on the pure (a-b) and single-Pd-doped Cu_{55} (c-h) nanoparticles.

nation number. Thus in our studies we calculated $E_{ad}(H)$ on the Cu(111) surface for comparison (Table 3). It was found that the adsorption energy of a single H atom on Cu(111) is 2.51 eV, either on an fcc or hcp site. This result agrees very well with previous calculations[39,40]. Compared to this value, the adsorption energy of H atom is 0.17 eV higher on the Cu_{55} nanoparticle. Therefore a higher temperature might be needed for the subsequent hydrogenation, and makes its selectivity reduced. We also considered the H atom adsorption on a larger cluster, that is, the 1.5-nm diameter Cu_{147} nanoparticle, the third Mackay icosahedron. It is interesting to find that the adsorption energy of the H atoms remarkably decreases on Cu_{147}, even lower than that on the Cu(111) surface (Table 3). Since a low activation energy of H_2 dissociation has been firmly confirmed at step sites, the result on Cu_{147} means that on nanoparticles one could achieve facile H_2 dissociation and weak H atom adsorption at the same time, indicating that the SAA concept is still workable at the nanoscale. Previous calculations have demonstrated that adsorption properties could change with size variation of the nanoparticles, and will approach to the bulk limits when size is large enough[41,42]. In our studies, the $E_{ad}(H)$ values could also change with the size of the Cu nanoparticles. The results on the Cu_{147} nanoparticle show that H atoms could be weakly bounded if the particle size is appropriate. It is reasonable to expect that such suitable range could match the size distribution of the nanoparticles under realistic conditions. A systematic investigation on the evolution of $E_{ad}(H)$ with Cu particle size will be extremely helpful to investigate this suitable range. Such study is beyond the scope of our present works and further efforts are needed to address this issue.

3.4 H Atom Diffusion on the Pure and Single-Pd-Doped Cu_{55} Nanoparticles

On the Pd-doped Cu(111) SAA surface, spillover of the H atom onto the Cu domain is essential to achieve its weak ad-

Table 1 The adsorption energies of H_2 molecule ($E_{ad}(H_2)$), the activation energies of H_2 dissociation ($E_b(disso)$), and the d band center of the Pd atom that bonds with the H_2 molecule (ε_d) for the configurations of pure and single-Pd-doped Cu_{55} nanoparticles. Energy barrier values with respect to the molecular well are also listed in the parentheses. The labels *a* and *b* in the parentheses correspond to the two dissociation pathways as shown in Figure 3. A positive value of $E_{ad}(H_2)$ represents an exothermic adsorption. The ε_d value is not shown if the H_2 molecule bonds with a Cu atom.

		$E_{ad}(H_2)$ (eV)	$E_b(disso)$ (eV)	ε_d (eV)
1Pd-doped Cu_{55}	Edge-Pd (a)	0.37	-0.01 (0.36)	-1.24
	Edge-Pd (b)	0.34	0.07 (0.41)	-1.24
	Top-Pd	0.30	0.65 (0.95)	-1.46
	Inner-Pd (a)	0.18	0.36 (0.54)	-
	Center-Pd (a)	0.09	0.51 (0.60)	-
pure Cu_{55}	Edge-Cu (a)	0.02	0.45 (0.47)	-
	Top-Cu	0.18	0.99 (1.17)	-

Table 2 The adsorption energies of a single H atom ($E_{ad}(H)$) on different sites of the pure (a-b) and single-Pd-doped Cu_{55} (c-h) nanoparticles (see Figure 5 for the configurations). Here $E_{ad}(H)$ is defined as: $E_{ad}(H) = E(NP) + E(H \text{ atom}) - E(NP-H)$.

| Sites	a	b	c	d	e	f	g	h
Types	fcc	hcp	fcc	hcp	hcp	hcp	hcp	hcp
$E_{ad}(H)$ (eV)	2.68	2.55	2.77	2.63	2.53	2.57	2.50	2.58

Table 3 The adsorption energies of a single H atom ($E_{ad}(H)$) on the Cu(111) surface and a larger Cu_{147} nanoparticle. The values on the Cu_{55} are also shown for comparison. Different from Cu_{55}, on Cu_{147} one of the hcp sites becomes the most stable adsorption site for the hydrogen atom.

	Sites	$E_{ad}(H)$ (eV)
Cu_{55}	fcc	2.68
	hcp	2.55
Cu(111)	fcc	2.51
	hcp	2.51
Cu_{147}	fcc	2.33
	hcp1	2.37
	hcp2	2.48

sorption after the facile H_2 dissociation. Therefore, the diffusion of the H atoms is important for the catalytic performance and should be investigated. We have calculated the diffusion barrier of the H atom on the pure and single-Pd-doped Cu_{55} nanoparticles, and compared the values with those on the corresponding extended surfaces (shown in Figure 6). The most stable adsorption site (see Table 2 and 3) is chosen to be the starting point of the diffusion path. One can see that on both cluster and surface systems the doping of a single Pd atom increases the value of the maximum H atom diffusion barrier that corresponds to the Pd-H bond breaking. The increment of the diffusion barrier comes from a stronger interaction

of Pd than Cu with the H atom, because of a higher-lying d states of Pd. Then we compared the H atom diffusion barrier on the nanoparticle with that on the extended surface. It is found that the diffusion barrier on the nanoparticle is a bit higher, which is originated from the lower atomic coordination number and the "ridge" configuration at the outermost layer of the nanoparticle. Notably, the H atom diffusion barrier is still lower than the H_2 adsorption energy, and is much lower than the energy release in the dissociative adsorption process. This means that the produced H atoms could gain enough energy for the following diffusion, and make this process energetically more favorable than the recombination of two H atoms. As a result, one can conclude that the slightly increment of the H atom diffusion barrier could not remarkably affect the spillover of the H atoms, and is not expected to significantly reduce the catalytic performance of the SAA nanoparticles, compared with that of the SAA surfaces.

Overall, by comparing the results between flat (111) surface and 55-atom nanoparticle, it is found that nanoparticle has lower activation energies for H_2 dissociation, while flat surface has lower H atom adsorption energies and diffusion barriers. Because of the trade-off between different reaction steps in the whole hydrogenation reaction, our results cannot determine which system, the surface or the nanoparticle, possess a better catalytic performance toward hydrogenation. Nevertheless, these results can demonstrate that the concept of single atom alloy could be workable at nanoscale.
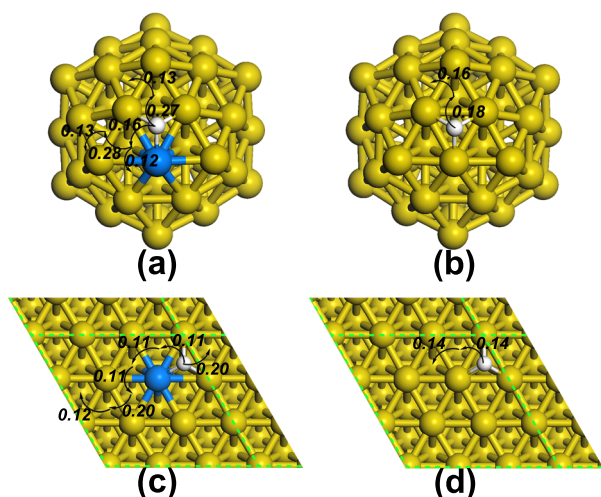
Fig. 6 The diffusion energy barrier of H atom on the single-Pd-doped Cu$_{55}$ (a), the pure Cu$_{55}$ (b), the single-Pd-doped Cu(111) surface (c) and the pure Cu(111) surface (d). The green dot line labels the unit cell of the extended surfaces in the calculations. The unit of the energy is eV.

3.5 The Effects of the Subsequent Pd Atom Doping

After addressing the effects of doping a single Pd atom into Cu$_{55}$ cluster, we have investigated the patterns of multiple Pd doping to explore the impact of the subsequent Pd atom on the catalytic properties toward hydrogenation. Because of the larger lattice constant of Pd, it could be anticipated that doping more Pd atoms will bring a greater distortion in the relaxed icosahedral nanoparticles. In our investigations, three different types of structures are taken into account, and the configurations are shown in Figure 7. The first type composes of one edge Pd atom at the shell and several contiguous Pd atoms in the inner layers of Cu$_{55}$. Owing to the unique core-shell structure of the Cu$_{55}$ cluster, there are up to two Pd atoms in the inner layer that could connect with the shell Pd atom at the edge site, shown as 'Pd2-E' and 'Pd3-E' in Figure 7. The second type contains two nearest-neighbour Pd atoms on the Cu$_{55}$ shell, shown as 'Pd2-S1' and 'Pd2-S2' in Figure 7. The third type of structures contains the Pd atoms that are randomly distributed at the cluster, shown as 'Pd2-R1' - 'Pd2-R4' in Figure 7. It is worth noting that the four structures of the type III are quite representative, because the second doping Pd atom occupies all the typical positions of Cu$_{55}$, for example, the edge and the top site at the shell, as well as the site in the inner layer.

Similarly, we first investigated the effect of subsequent Pd atom doping on the activation energy of H$_2$ dissociation. From Table 4 one can see that with the substitution of the connected inner-Pd atoms, the activation energy of the H$_2$ dissociation
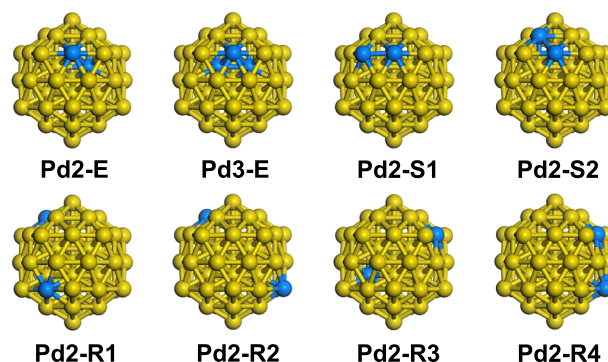

Fig. 7 Structures of the doped Cu$_{55}$ nanoparticles with multiple Pd atoms substitution. The abbreviation "E" represents the connected Pd ensemble composed of Pd atoms in both the outer and the inner layers. "S" represents the structure having connected Pd atoms at the surface layer. "R" refers to the structure with a random distribution of the doping Pd atoms.

becomes as low as -0.20 eV on the configuration of 'Pd2-E' and -0.28 eV on that of 'Pd3-E'. Compared to the value of -0.01 eV on the single-Pd-doped Cu$_{55}$ (Figure 3), the activation energy of H$_2$ dissociation is remarkably decreased. It is reminiscent of the fact that on the flat and stepped Cu(111) surfaces, a small number of subsurface Pd atoms can effectively reduce the activation energy of the H$_2$ dissociation[23]. It is also interesting to see that the Pd ensemble composed of the shell and the contiguous inner Pd atoms exhibit a lower dissociation activation energy on the 55-atom nanoparticle than that on the extended surfaces (0.05 eV on (111) and -0.09 eV on (211) surface, respectively). However, it should be noted that the value of a negative activation energy is not as meaningful as that of a positive one for kinetics. Actually a negative value just means that the corresponding reaction step could occur spontaneously; but here a lower value of activation energy does not mean a better catalytic activity. For the configurations that contain two nearest-neighbour Pd atoms ('Pd2-S1' and 'Pd2-S2'), we found that the activation energy of H$_2$ dissociation is the same, that is, -0.06eV for both the nearest-neighbour arrangements. Compared with the value on the single-Pd-doped Cu$_{55}$ (-0.01 eV), the activation energy only slightly decreases. For the third type structures, that is, the ones with the two Pd atoms separated from each other, the second doping Pd atom has almost no effect on the activation energy of the H$_2$ dissociation, which means that the edge Pd atoms can independently dissociate the incoming H$_2$ molecules.

The different values of activation energy for H$_2$ dissociation come from the differences of the electronic structure in various configurations. According to the famous *d* band model[2–4], the interaction strength between the transition metal sur-

Table 4 The adsorption energies of H_2 molecule ($E_{ad}(H_2)$), the activation energies of H_2 dissociation (E_b(disso)) and the d band center of the Pd atom that bonds with the H_2 molecule (ε_d) for the configurations with multiple Pd doping as shown in Figure 7. Energy barrier values with respect to the molecular well are also listed in the parentheses.

	$E_{ad}(H_2)$ (eV)	E_b(disso) (eV)	ε_d (eV)
Pd2-E	0.48	-0.20 (0.28)	-1.17
Pd3-E	0.54	-0.28 (0.26)	-1.05
Pd2-S1	0.34	-0.06 (0.28)	-1.24
Pd2-S2	0.37	-0.06 (0.31)	-1.21
Pd2-R1	0.34	0.03 (0.37)	-1.30
Pd2-R2	0.36	-0.03 (0.33)	-1.31
Pd2-R3	0.35	0.03 (0.38)	-1.29
Pd2-R4	0.36	-0.02 (0.34)	-1.29
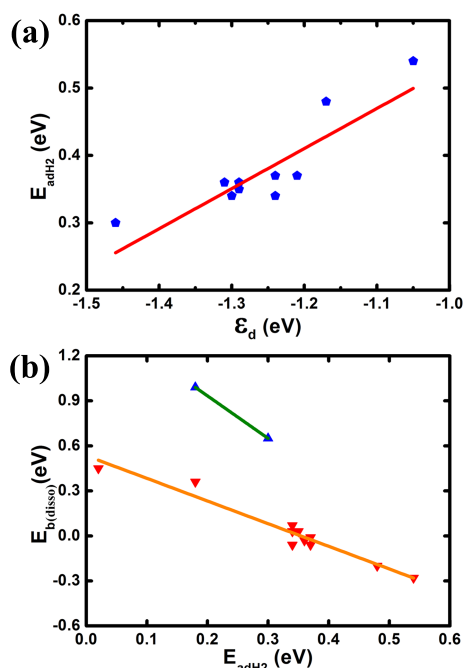
Fig. 8 (a) Correlation relation between d band center of the Pd atom that connects with H_2 molecule (ε_d) and the corresponding H_2 adsorption energy (E_{adH2}). (b) Correlation relation between activation energy of H_2 dissociation (E_b(disso)) and H_2 adsorption energy (E_{adH2}). The green line (blue triangle) refers to the dissociation at the top site, while the orange line (red triangle) represents that at the edge site.

face and the adsorbate is correlated with the energy average of the d electrons, that is, the d band center ε_d. It was found that the upshift of ε_d corresponds to an increment of the adsorption energy [2–4]. Recently, this useful relation was also applied in Pd/Cu bimetallic nanoparticles to tune their catalytic activity toward oxygen reduction reaction [43,44]. In Table 1 and Table 4 we listed the ε_d values for the various configurations of nanoparticles. The correlation between the H_2 adsorption energy and these ε_d values is shown in Figure 8a. One can see that the H_2 adsorption energy increases with the upshift of the ε_d value, in a similar way as what we have found on the flat and stepped Pd-doped Cu(111) surfaces [23]. From our previous studies we have known that the increment of the H_2 adsorption energy, which comes from the upshift of the ε_d value, stabilizes the molecular well as well as the transition state, and results in the reduction of H_2 dissociation activation energy [23]. According to the results in Table 1 and Table 4, only the connected inner-Pd atoms could effectively move up the ε_d value and increase the H_2 adsorption energy, which explains the lower H_2 activation energy on these configurations. Besides, it is interesting to find that the ε_d of the Pd atom at the top site (Top-Pd, -1.46 eV) is lower than that at the edge site (Edge-Pd, -1.24 eV), although the Top-Pd has a lower coordination number. It is worth noting that the atom with a lower coordination number usually has a upper ε_d value [3,4], responsible for its higher activity often appearing on the nanoparticles and the stepped surfaces. This interesting phenomenon comes from a joint action from two aspects of the geometric effects. On one hand, a lower coordination number of the top-Pd atom could indeed result in an up-shift of the d band center, as had been mentioned above. On the other hand, because of the special doping site, the Pd atom at the edge site induces a significant deformation of the nearby Cu atoms (Figure 2), and makes its d band center move even higher. As a result, the edge-Pd atom with a larger coordination number has a higher d band center.

In Figure 8b, the activation energy of H_2 dissociation against the H_2 adsorption energy is plotted. One can see that the activation energy decreases with the increment of the adsorption energy, which is reminiscent of the similar relations on the flat and stepped Pd-doped Cu(111) surfaces [23]. It indicates that the more-easily-calculated H_2 adsorption energy can be used as the "descriptor" to estimate the activity of the Pd-doped Cu_{55} cluster toward H_2 dissociation. Depending on the doping pattern of the Pd atoms, the data in Figure 8 can be divided into two groups. It comes from the difference in the local configurations of the Pd atoms (top and edge site). The large distance between the two straight lines reflects a stronger geometric effect in the correlation relations [45,46].

After the issue of H_2 dissociation has been addressed, we then investigated the effect of the subsequent Pd atom on the H atom adsorption energy. For each doping pattern of Pd several

Table 5 The maximum adsorption energy of the H atoms (E_{ad}^{max}(H)) for the configurations with multiple Pd doping as shown in Figure 7. The corresponding value on the single-Pd-doped Cu$_{55}$ is also listed for comparison.

	E_{ad}^{max}(H) (eV)
Edge-Pd	2.77
Pd2-E	2.76
Pd3-E	2.77
Pd2-S1	2.71
Pd2-S2	2.84
Pd2-R1	2.73
Pd2-R2	2.75
Pd2-R3	2.73
Pd2-R4	2.74

Table 6 The excess energies E_{exc}(Vac) and E_{exc}(H$_2$) for the various Pd-doped Cu$_{55}$ nanoparticles.

	E_{exc}(Vac) (eV)	E_{exc}(H$_2$) (eV)
Edge-Pd	-0.52	-0.89
Top-Pd	-0.49	-0.78
Inner-Pd	-0.12	-0.30
Center-Pd	0.17	0.08
Pd2-E	-0.58	-1.06
Pd2-S1	-0.90	-1.25
Pd2-S2	-0.97	-1.34
Pd2-R1	-1.12	-1.46
Pd2-R2	-1.08	-1.44
Pd2-R3	-0.71	-1.05
Pd2-R4	-1.05	-1.41

adsorption sites for the H atom have been considered. Here we mainly focus on the maximum adsorption energy(E_{ad}^{max}(H)), because if such value is not increased by the subsequent doping Pd atom, the spillover of H atoms will not be hindered by this Pd atom either. From the calculation results listed in Table 5, one can see that the H atom adsorption will not be enhanced by the doping of the subsequent Pd atom, except in the case of 'Pd2-S2', where the E_{ad}^{max}(H) value increases by 0.07 eV.

3.6 Stability

The stability of the various Pd doping patterns is another important issue that should be carefully addressed, because the Pd configuration can directly affect the activation energy of H$_2$ dissociation and the H atom adsorption. Thanks to the highly symmetrical structure of the icosahedral Cu$_{55}$ and the ultra low doping concentration of Pd (a single Pd atom), in our studies it is possible to enumerate the different configurations of Pd for the stability analysis. For more complex structures and doping modes, enumeration is no longer applicable. It is worth noting that there is a systematic method to explore all the stable alloy configurations for nanoparticles[47,48], which can be used as a systematic approach to investigate the crucial structural information for nanoalloy catalysis.

Here we use the values of excess energy[49,50], defined in eq 1, to estimate the thermodynamic stability of the bimetallic nanocluster with different Pd substitutions. The abbreviation 'Vac' indicates that the E_{exc} value is calculated in the vacuum, without the effects of the surrounding adsorbates. The $E_{Pd_{55}}$ and $E_{Cu_{55}}$ is the energy of the icosahedral Pd$_{55}$ and Cu$_{55}$ cluster respectively. A negative value of E_{exc} represents an exothermic alloying process.

$$E_{exc}(Vac) = [E_{Pd_nCu_{55-n}} - n \times \frac{E_{Pd_{55}}}{55} - (55-n) \times \frac{E_{Cu_{55}}}{55}] \quad (1)$$

It is worth noting that the configuration of an alloy system can also be affected by the realistic reaction conditions. For example, both experimental[51-53] and theoretical[16,17,54] studies have shown that the adsorbate can induce surface segregation, which comes from a stronger interaction with some particular elements. As a result, the effects of H$_2$ environment on the stability of nanoparticles should be taken into account. Here we adopt a modified formula for the excess energy, as given in eq 2, to consider the effects of the H$_2$ adsorbates.

$$E_{exc}(H_2) = [E_{Pd_nCu_{55-n}-adH_2} - E(H_2) - n \times \frac{E_{Pd_{55}}}{55}$$
$$- (55-n) \times \frac{E_{Cu_{55}}}{55}] \quad (2)$$

The E(H$_2$) is the energy of an isolated hydrogen molecule, and $E_{Pd_nCu_{55-n}-adH_2}$ is the energy of the nanoparticles after H$_2$ adsorption.

The calculated results of the E_{exc}(Vac) and E_{exc}(H$_2$) are listed in Table 6. For the single-Pd-doped Cu$_{55}$ nanoparticle, the configuration of 'Edge-Pd' has the lowest excess energy (-0.52 eV), which means that such configuration is the most stable one. The structure of 'Center-Pd', however, has a positive and the largest excess energy (0.17 eV), indicating that such doping pattern is energetically unfavorable. It is interesting to find that among all the doping patterns by a single Pd atom, the structure of 'Edge-Pd', the one with the lowest activation energy of H$_2$ dissociation, is actually the most stable configuration. In addition, its stability can be further improved by the surrounding H$_2$ environment owing to a stronger interaction between the nanoparticle and the H$_2$ molecule.

It is interesting to discuss how to achieve the doping site of 'Edge-Pd' and exclude all the others in experiments. Since the radius of Pd atom (169pm) is larger than that of Cu (145pm)[55], doping Pd atoms in inner layers of Cu nanoparticle is

unfavorable from a thermodynamic point of view. As a result, inner doping sites can easily be avoided just by heating to promote the segregation of Pd atoms. For Pd atoms on the shell of nanoparticles, in vacuum the 'Edge-Pd' atom is only slightly more stable (0.03 eV) than the 'Top-Pd' atom. Under H_2 atmosphere, however, the energy difference increases to 0.11 eV, which means that H_2 environment can be used to stabilize the active 'Edge-Pd' doping sites. Moreover, in order to increase the atom efficiency of expensive Pd element, the doping Pd atoms should be kept at a low concentration in the synthesis, following the strategy of single atom alloy. Overall, to achieve the active 'Edge-Pd' doping sites in experiments, it is suggested to use a low concentration of Pd atoms, to anneal the nanoparticles, and to place the nanoparticles under H_2 atmosphere.

From Table 6 one can see that for the configuration with two doping Pd atoms (Table 6), the structure of 'Pd2-R1', where both Pd atoms locate at the edge sites, has the lowest E_{exc} value, even lower than twice of the E_{exc} value for a single Edge-Pd atom (-1.04 eV). These two doping Pd atoms in the configuration of 'Pd2-R1' could independently exhibit their catalytic activity as the active site, meaning that the structure of 'Pd2-R1', containing two doping Pd atoms, can actually behave as two single-atom-alloy catalysts.

4   Conclusions

To conclude, our first-principles calculations have shown that doping a single Pd atom at the edge site can remarkably decrease the activation energy of H_2 dissociation on Cu_{55} nanoparticle. Although the adsorption of the resulting H atoms is slightly enhanced compared with Cu(111), a larger nanoparticle containing 147 atoms is found to recover the weak binding. Besides, the spillover of the H atoms is found to be feasible thanks to the low diffusion barriers. Overall, our results demonstrate the effectiveness of the single atom alloy concept at the nanoscale, and would shed new light on the catalytic properties of nanoalloy systems.
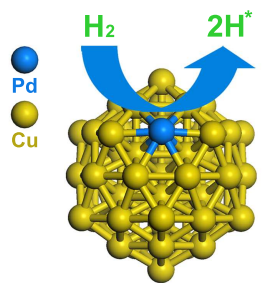
Acknowledgement

References

1 M. Beller and C. Bolm, *Transition Metals for Organic Synthesis: Building Blocks and Fine Chemicals*, WILEY-VCH Verlag GmbH & Co. KGaA, Weinheim, 2nd edn, 2004.
2 B. Hammer and J. K. Nørskov, *Nature*, 1995, **376**, 238–240.
3 B. Hammer and J. K. Nørskov, *Adv. Catal.*, 2000, **45**, 71–129.
4 B. Hammer, *Top. Catal.*, 2006, **37**, 3–16.
5 V. R. Stamenkovic, B. Fowler, B. S. Mun, G. Wang, P. N. Ross, C. A. Lucas and N. M. Marković, *Science*, 2007, **315**, 493–497.
6 J. Y. Park, Y. Zhang, M. Grass, T. Zhang and G. A. Somorjai, *Nano Lett.*, 2008, **8**, 673–677.
7 S. Alayoglu, A. U. Nilekar, M. Mavrikakis and B. Eichhorn, *Nat. Mater.*, 2008, **7**, 333–338.
8 H. Lee, S. E. Habas, G. A. Somorjai and P. Yang, *J. Am. Chem. Soc.*, 2008, **130**, 5406–5407.
9 D. Xu, S. Bliznakov, Z. Liu, J. Fang and N. Dimitrov, *Angew. Chem. Int. Ed.*, 2010, **49**, 1282–1285.
10 H. Zhang, T. Watanabe, M. Okumura, M. Haruta and N. Toshima, *Nat. Mater.*, 2012, **11**, 49–52.
11 J. G. Chen, C. A. Menning and M. B. Zellner, *Surf. Sci. Rep.*, 2008, **63**, 201–254.
12 J. K. Nørskov, T. Bligaard, B. Hvolbaek, F. Abild-Pedersen, I. Chorkendorff and C. H. Christensen, *Chem. Soc. Rev.*, 2008, **37**, 2163–2171.
13 T. Bligaard and J. K. Nørskov, *Chemical Bonding at Surfaces and Interfaces*, Elsevier, Amsterdam, 2008.
14 J. K. Nørskov, T. Bligaard, J. Rossmeisl and C. H. Christensen, *Nat. Chem.*, 2009, **1**, 37–46.
15 J. K. Nørskov, F. Abild-Pedersen, F. Studt and T. Bligaard, *Proc. Natl. Acad. Sci.*, 2011, **108**, 937–943.
16 J. Greeley and M. Mavrikakis, *Nat. Mater.*, 2004, **3**, 810–815.
17 J. Greeley and M. Mavrikakis, *Catal. Today*, 2006, **111**, 52–58.
18 L. C. Grabow, *Chem. Cat. Chem.*, 2012, **4**, 1887–1888.
19 H. L. Tierney, A. E. Baber, J. R. Kitchin and E. C. H. Sykes, *Phys. Rev. Lett.*, 2009, **103**, 246102.
20 D. O. Bellisario, J. W. Han, H. L. Tierney, A. E. Baber, D. S. Sholl and E. C. H. Sykes, *J. Phys. Chem. C.*, 2009, **113**, 12863–12869.
21 H. L. Tierney, A. E. Baber and E. C. H. Sykes, *J. Phys. Chem. C.*, 2009, **113**, 7246–7250.
22 G. Kyriakou, M. B. Boucher, A. D. Jewell, E. A. Lewis, T. J. Lawton, A. E. Baber, H. L. Tierney, M. Flytzani-Stephanopoulos and E. C. H. Sykes, *Science*, 2012, **335**, 1209–1212.
23 Q. Fu and Y. Luo, *ACS Catal.*, 2013, **3**, 1245–1252.
24 M. B. Boucher, B. Zugic, G. Cladaras, J. Kammert, M. D. Marcinkowski, T. J. Lawton, E. C. H. Sykes and M. Flytzani-Stephanopoulos, *Phys. Chem. Chem. Phys.*, 2013, **15**, 12187–12196.
25 P. E. Blöchl, *Phys. Rev. B*, 1994, **50**, 17953–17979.
26 J. P. Perdew and Y. Wang, *Phys. Rev. B*, 1992, **45**, 13244–13249.
27 G. Henkelman, B. P. Uberuaga and H. Jónsson, *J. Chem. Phys.*, 2000, **113**, 9901–9904.
28 G. Henkelman and H. Jónsson, *J. Chem, Phys.*, 1999, **111**, 7010–7022.
29 G. Kresse and J. Furthmüller, *J. Comput. Mater. Sci.*, 1996, **6**, 15–50.
30 G. Kresse and J. Furthmüller, *Phys. Rev. B*, 1996, **54**, 11169.
31 Z. L. Wang, *J. Phys. Chem. B.*, 2000, **104**, 1153–1175.
32 Y. Xiong, B. J. Wiley and Y. Xia, *Angew. Chem., Int. Ed.*, 2007, **46**, 7157–7159.
33 V. G. Grigoryan, D. Alamanova and M. Springborg, *Phys. Rev. B.*, 2006, **73**, 115415.
34 H. Häkkinen, M. Moseler, O. Kostko, N. Morgner, M. A. Hoffmann and B. v. Issendorff, *Phys. Rev. Lett.*, 2004, **93**, 093401.
35 T. Rapps, R. Ahlrichs, E. Waldt, M. M. Kappes and D. Schooss, *Angew. Chem. Int. Ed.*, 2013, **52**, 6102–6105.

36 J. E. Lennard-Jones, *Trans. Faraday Soc.*, 1932, **28**, 333–359.

37 M. Ramos, A. E. Martinez and H. F. Busnengo, *Phys. Chem. Chem. Phys.*, 2012, **14**, 303–310.

38 B. Yang, X.-Q. Gong, H.-F. Wang, X.-M. Cao, J. J. Rooney and H. P., *J. Am. Chem. Soc.*, 2013, **135**, 15244–15250.

39 M. F. Luo, H. G. R. and L. M. H., *Surf. Sci.*, 2007, **601**, 1461–1466.

40 P. Ferrin, S. Kandoi, A. U. Nilekar and M. Mavrikakis, *Surf. Sci.*, 2012, **606**, 679–689.

41 J. Kleis, J. Greeley, N. A. Romero, V. A. Morozov, H. Falsig, A. H. Larsen, J. Lu, J. J. Mortensen, M. Dułak, K. S. Thygesen, J. K. Nørskov and K. W. Jacobsen, *Catal. Lett.*, 2011, **141**, 1067–1071.

42 L. Li, A. H. Larsen, N. A. Romero, V. A. Morozov, C. Glinsvad, F. Abild-Pedersen, J. Greeley, K. W. Jacobsen and J. K. Nørskov, *J. Phys. Chem. Lett.*, 2013, **4**, 222–226.

43 W. Tang, L. Zhang and G. Henkelman, *J. Phys. Chem. Lett.*, 2011, **2**, 1328–1331.

44 L. Zhang and G. Henkelman, *J. Phys. Chem. C.*, 2012, **116**, 20860–20865.

45 J. K. Nørskov, T. Bligaard, B. Hvolbaek, F. Abild-Pedersen, I. Chork-endorff and C. H. Christensen, *Chem. Soc. Rev.*, 2008, **37**, 2163–2171.

46 Q. Fu, X. R. Cao and Y. Luo, *J. Phys. Chem. C*, 2013, **117**, 2849–2854.

47 L.-L. Wang, T. L. Tan and D. D. Johnson, *Phys. Rev. B*, 2012, **86**, 035438.

48 T. L. Tan, L.-L. Wang, D. D. Johnson and K. Bai, *Nano. Lett.*, 2012, **12**, 4875–4880.

49 R. Ferrando, A. Fortunelli and G. Rossi, *Phys. Rev. B*, 2005, **72**, 085449.

50 X. Liu, D. Tian and C. Meng, *Chem. Phys.*, 2013, **415**, 179–185.

51 J. A. Anderson, M. Fernández-García and G. L. Haller, *J. Catal.*, 1996, **164**, 477–483.

52 F. Tao, M. E. Grass, Y. Zhang, D. R. Butcher, J. R. Renzas, Z. Liu, J. Y. Chung, B. S. Mun, M. Salmeron and G. A. Somorjai, *Science*, 2008, **322**, 932–934.

53 D. Priyadarshini, P. Kondratyuk, Y. N. Picard, B. D. Morreale, A. J. Gell-man and J. B. Miller, *J. Phys. Chem. C*, 2011, **115**, 10155–10163.

54 Q. Fu and Y. Luo, *J. Phys. Chem. C*, 2013, **117**, 14618–14624.

55 E. Clementi, D. L. Raimondi and W. P. Reinhardt, *J. Chem. Phys.*, 1967, **47**, 1300–1307.

Single Atom Nanoalloy